Journal of Alloys and Compounds 509 (2011) 6170–6174

Contents lists available at ScienceDirect

Journal of Alloys and Compounds

journal homepage: www.elsevier.com/locate/jallcom

Phase transformation in Mg–8Gd–4Y–Nd–Zr alloy

Xin-ming Zhang[a,b,*], Chang-ping Tang[a,b], Yun-lai Deng[a,b], Liu Yang[a,b], Wen-jun Liu[a,b]

[a] School of Materials Science and Engineering, Central South University, Changsha 410083, PR China
[b] The Key Laboratory of Nonferrous Metal Materials Science and Engineering, Ministry of Education, Changsha 410083, PR China

ARTICLE INFO

Article history:
Received 26 November 2010
Received in revised form 5 March 2011
Accepted 8 March 2011
Available online 16 March 2011

Keywords:
Alloy
Precipitation
DSC
Temperature
Activation energy

ABSTRACT

Precipitation reactions in a Mg–8Gd–4Y–Nd–Zr alloy were investigated using hardness measurements, TEM and DSC, and a four stage precipitation sequence determined: Mg (SSSS) → β″ → β′ → β_1 → β. Thermal effect signals in the DSC curves due to the formation of the β″, β′, β_1 and β phases and the dissolution of the β″ phase were identified. The activation energies associated with the formation of the β′ and β_1/β phases were determined according to the Kissinger method. These kinetic parameters were related to the heat-resistant mechanism of the Mg–8Gd–4Y–Nd–Zr alloy.

1. Introduction

Precipitation hardened magnesium–rare earth (RE) alloys, due to their attractive mechanical properties at both room temperature and elevated temperature, have been widely used in the aerospace and racing automotive industries [1]. The precipitation reactions in the Mg–RE-based alloys, particularly those based on the Mg–Y–Nd and Mg–Gd–Y systems, during isothermal ageing, have attracted considerable attention [2–7], and a four stage precipitation sequence of Mg (SSSS) → β″ → β′ → β_1 → β has been proposed [4,5,8]. The morphology and the composition of these phases have also been discussed [3,9–12]. Moreover, as a heat-resistant magnesium alloy system, studies of the precipitation kinetics have become important for further development. However, kinetic data such as activation energies in the Mg–Gd–Y–Zr alloy system have rarely been investigated.

Differential scanning calorimetry (DSC) is particularly useful for following phase transformations as the temperature increases. More recently, studies indicated that DSC can provide both qualitative and quantitative descriptions of the phase transformations in alloys [2,13–17]. The activation energies can be obtained from the shift of peak temperatures with changes in the heating rate in non-isothermal scans. In the present work, the phase transformations in the Mg–8Gd–4Y–Nd–Zr alloy were investigated and they were associated with the exothermic and endothermic reactions in the DSC traces. The activation energies for phase transformations were obtained and the heat-resistant mechanism was discussed as well.

2. Experimental procedures

An alloy ingot with a nominal composition of Mg–8.0Gd–4.0Y–1.0Nd–1.0Zr (wt.%) was prepared from high purity Mg (>99.93%), Mg–31.25Gd (wt.%), Mg–25.48Y (wt.%), Mg–30.15Nd (wt.%) and Mg–30.23Zr (wt.%) master alloys by melting in a mild steel crucible at 760 °C under argon atmosphere. The actual chemical composition of the ingot was determined to be Mg–7.71Gd–3.45Y–1.02Nd–0.51Zr (wt.%). The ingot was quenched into cold water after solution heat treatment at 520 °C for 12 h, and then it was cut into 15 mm × 15 mm × 2 mm pieces for ageing. Hardness tests were performed with a HV-10B type Vickers microindenter and a load of 30 N; the reported values in this paper are the average of nine indentations. Calorimetric scans were carried out on specimens with a diameter of about 5 mm and 40 mg in mass, with a NETZSCH DSC 200 F3 apparatus under protective pure argon atmosphere. The testing was performed at different heating rates and pure magnesium was employed as a reference. The samples for transmission electron microscopy tests were ion milled using the Precision Ion Polishing System (GATAN 691). Microstructure observations were performed with a Tecnai G2 20 transmission electron microscope.

3. Results and discussion

3.1. DSC traces and phase analysis

The DSC trace after baseline subtraction of the as-quenched (AQ) sample is shown in Fig. 1. Three main processes can be identified from the DSC curve as indicated by signals A, B and C, while the specific phase transformation processes are still unclear. In the initial stage, signal A was rather extended in temperature, which

* Corresponding author at: School of Materials Science and Engineering, Central South University, Changsha 410083, PR China. Tel.: +86 073188830265; fax: +86 073188830265.
E-mail addresses: tangcpswnu@sina.com, tcpswnu@163.com, xmzhang_cn@yahoo.cn (X.-m. Zhang).

0925-8388/$ – see front matter © 2011 Elsevier B.V. All rights reserved.
doi:10.1016/j.jallcom.2011.03.059

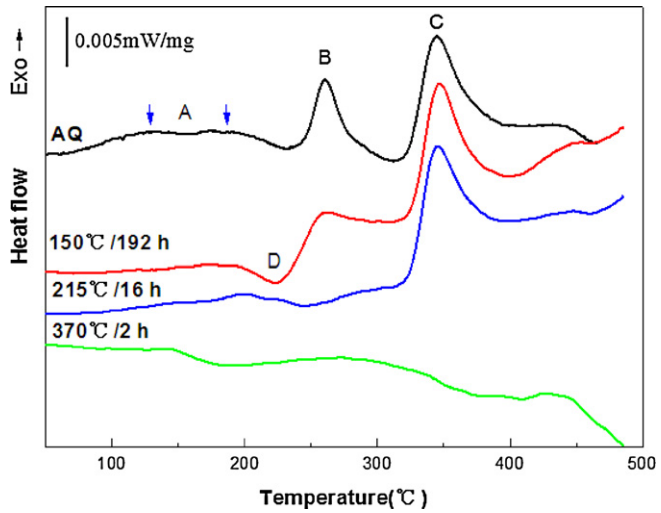

Fig. 1. DSC traces after baseline subtraction of the samples with different initial states (Scanning rate: 1 °C/min).

was also observed in other alloys containing rare earth elements [2,13–17]. This phenomenon may be due to the overlapping of different phase transformation processes. Actually, it seems to include two exothermic signals, as the arrows in Fig. 1 show.

In order to correlate the three main signals to specific processes, samples were chosen to age at temperatures ranging from 150 °C to 370 °C according to the DSC curve of the as-quenched sample. DSC testing was also performed on some pre-aged samples, such as the 150 °C/192 h-, 215 °C/16 h- and 370 °C/2 h-aged samples, which represent the under-, peak- and over-aged states, respectively. The pre-aged samples also correspond to different precipitation states.

Compared to the curve of the as-quenched sample, the main distinct features of the DSC curve of the 150 °C/192 h-aged sample were the exothermic signal A that almost disappeared and the observed endothermic signal D. It is suggested that the phases precipitated during the pre-ageing process decreased the precipitation tendency, and some existing precipitates dissolved during scanning.

Fig. 2 shows the hardness curve of the samples aged at 150 °C. The hardness increased gently and did not reach the peak within 192 h. It was just 96 VHN after ageing at 150 °C for 192 h, and increased only 17% compared with the as-quenched sample (82 VHN). Fig. 3a shows the TEM image of the sample aged at 150 °C

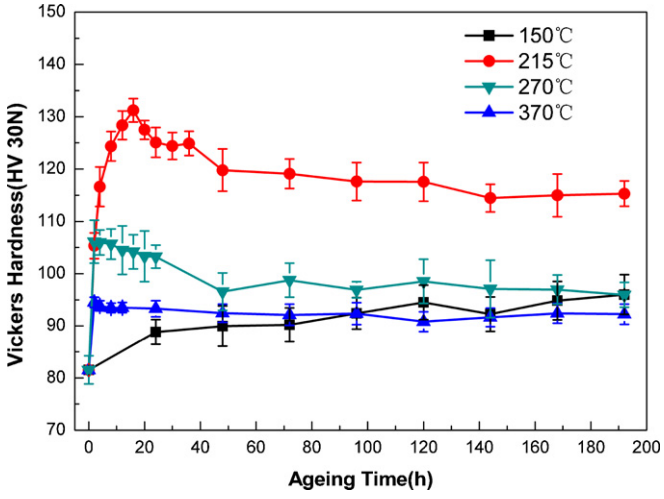

Fig. 2. Hardness evolution as a function of ageing time during isothermal ageing at different temperatures.

for 192 h that has plenty of fine precipitates. The electron diffraction pattern recorded along the $\langle 0\,0\,0\,1\rangle_{Mg}$ zone axis is shown in Fig. 3b. Diffuse spots are present at half distance of the $\{1\,0\,\bar{1}\,0\}$ Mg reflections. These patterns were consistent with that of the DO_{19} structure, and the lattice parameters of this phase are $a = 2a_{\alpha\text{-Mg}} \approx 0.64$ nm, $c = c_{\alpha\text{-Mg}} \approx 0.52$ nm. The orientation relationship between the precipitate and the matrix was determined to be $[0\,0\,0\,1]_{\beta''} \| [0\,0\,0\,1]_{\alpha}$, $[2\,\bar{1}\,\bar{1}\,0]_{\beta''} \| [2\,\bar{1}\,\bar{1}\,0]_{\alpha}$. Such features are typical in Mg–RE-based alloys [3,4,7,11]. This precipitate apparently formed at the initial stage of ageing, and it was fully coherent with the matrix. Therefore, the continuous increase of hardness can be attributed to the formation of the β″ phase, and it is reasonable to conclude that the endothermic signal D in the DSC curve was associated with the dissolution of the β″ phase. The disappearance of signal A may be attributed to the decrease in the supersaturation of the matrix, which led to a decrease in the driving force for precipitation during scanning.

Compared to the DSC curves of the as-quenched and the 150 °C/192 h-aged samples, only the exothermic signal C existed in the DSC curve of the 215 °C/16 h-aged sample (Fig. 1). This suggests that no phases precipitated or dissolved at temperatures lower than 300 °C during the DSC scan. The hardness evolution of the samples aged at 215 °C is shown in Fig. 2. In the initial stage, the hardness of the samples increased rapidly and reached their peak shortly (16 h), and then decreased gradually. The TEM image of the sample aged at 215 °C for 16 h (peak-aged) revealed a high number density of plate-shaped precipitates (Fig. 4a). These precipitates were determined to be β′ precipitates according to the SAED pattern shown in Fig. 4b. The orientation relationship between the precipitate and the matrix was $[0\,0\,1]_{\beta'} \| [0\,0\,0\,1]_{\alpha}$ and $(1\,0\,0)_{\beta'} \| (2\,\bar{1}\,\bar{1}\,0)_{\alpha}$. These plate-shaped precipitates were also observed in other peak-aged Mg–Gd–Y–Zr alloys [11,18], and they were considered to be the most effective strengthening phase lying in the $\{1\,1\,\bar{2}\,0\}_{\alpha}$ plane. Therefore, the steep growth of the hardness when aged at 215 °C was ascribed to the formation of these plate-shaped precipitates. As plenty of β′ precipitates have precipitated from the matrix, the supersaturation of the matrix decreased dramatically, which lowered the driving force for precipitating the β″ and β′ phases during scanning and resulted in the disappearance of the signals A and B in the DSC curve of the 215 °C/16 h-aged sample. Thus, it is reasonable to conclude that the exothermic signal B is due to the precipitation of the β′ phase. Moreover, there are no β″ precipitates in the peak-aged (215 °C/16 h) sample, which lead to the disappearance of the endothermic signal D in the DSC curve.

In order to correlate a specific process with signal C, selected samples were aged at higher temperatures. When the samples were aged at 370 °C, the hardness initially increased and finally stabilized at a value 15% higher than the initial hardness (Fig. 2). After aged at 370 °C for 2 h, coarse precipitates of about 2 μm (Fig. 5a) were observed, which were determined to be the equilibrium β phase based on the SAED pattern shown in Fig. 5b. These equilibrium precipitates were incoherent with the matrix, and their strengthening effect was limited according to the well-known Orowan mechanism [19]. Apparently, it was the main reason for the low-level stabilization of the hardness value.

The β_1 phase has been reported in many other rare earth containing alloys [3–8,14]. It was observed to nucleate at the interface of the β′ precipitates with the matrix, and it will transform in situ to the equilibrium β phase. In order to establish whether there was β_1 phase in the Mg–8Gd–4Y–Nd–Zr alloy, samples were chosen to age at 270 °C. The hardness curve is shown in Fig. 2. It revealed that the hardness curve of the 270 °C-aged samples shared similar trend with that of 215 °C-aged samples but the former reached the peak in just 2 h. The TEM image taken approximately parallel to the $\langle 0\,0\,0\,1\rangle_{Mg}$ is shown in Fig. 6a. It shows that there were two different phases, which were identified as the β′ and β_1 phase. The elec-

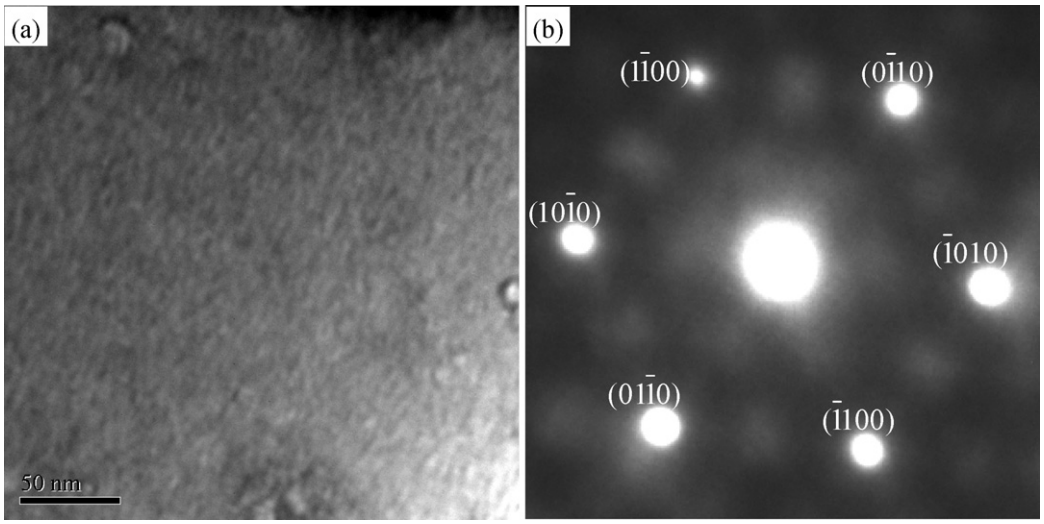

Fig. 3. Transmission electron micrograph (a) and the diffraction pattern recorded from [0 0 0 1] (b) of the sample aged at 150 °C for 192 h.

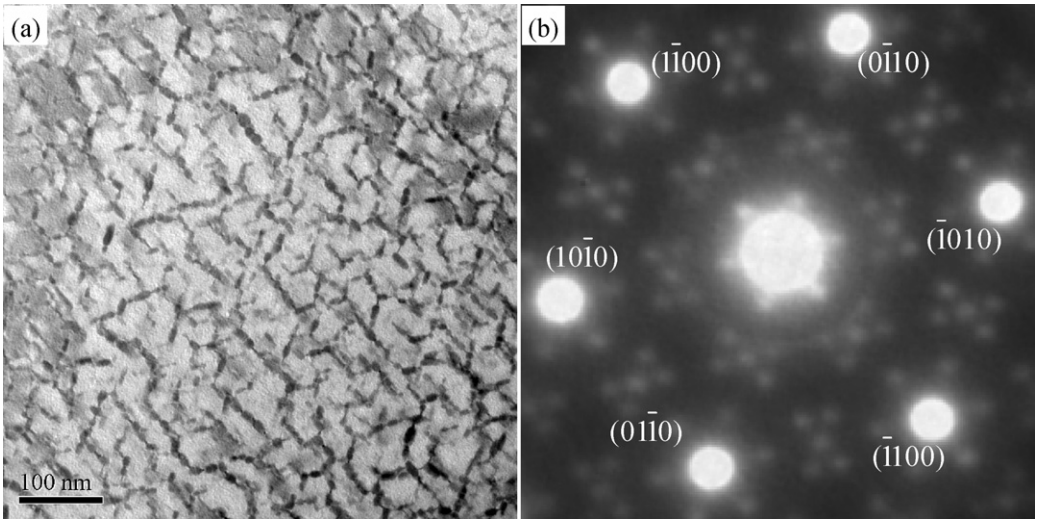

Fig. 4. TEM image (a) of the sample aged at 215 °C for 16 h and the SAED pattern (b) recorded from [0 0 0 1].

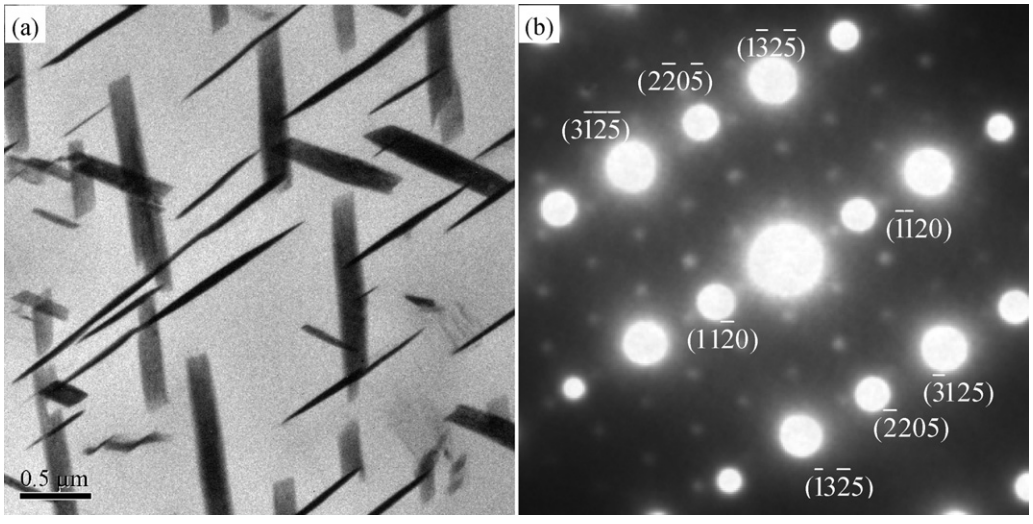

Fig. 5. TEM image (a) and the SAED pattern recorded from [5 $\bar{5}$ 0 4] (b) of the sample aged at 370 °C for 2 h.

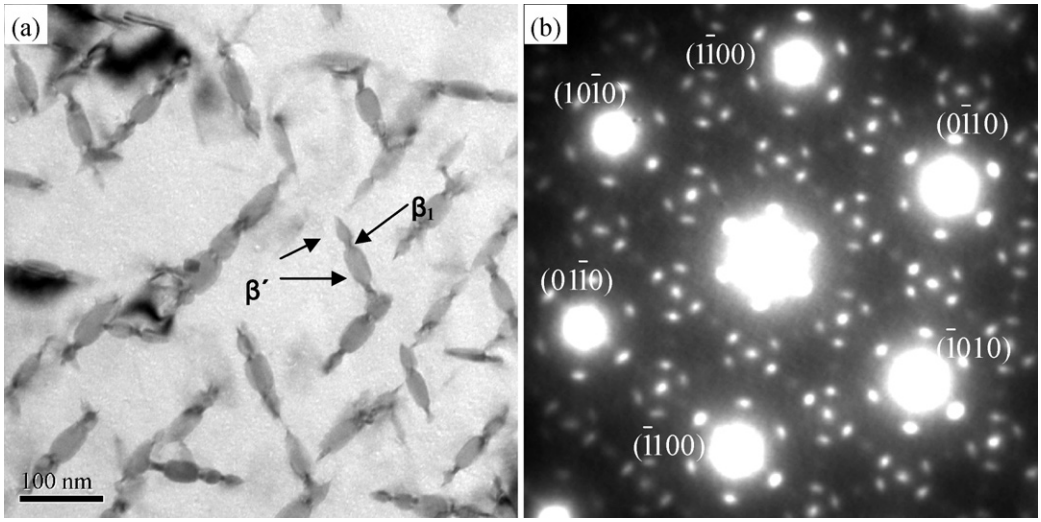

Fig. 6. Bright field image (a) and the SAED pattern recorded from [0 0 0 1] zone axis (b) of the sample aged at 270 °C for 2 h.

tron diffraction pattern in Fig. 6b showed extra spots besides the diffraction pattern of the β′ precipitates that were connected by the plate-shaped β_1 precipitates in accordance with the observation of other researchers [4,5,7,8,14].

The DSC curve of the 370 °C/2 h-aged sample showed no evident exothermic and endothermic signals (Fig. 1). Thus, according to the DSC and the TEM results, it can be concluded that the metastable β_1 phase existed between the β′ and the equilibrium β phases in the Mg–8Gd–4Y–Nd–Zr alloy, and the exothermic signal C is due to the precipitation of β_1 and β phases.

3.2. Transformation kinetics

The calorimetric signals B and C for the as-quenched sample were well separated, which made it possible for us to obtain the activation energy of the phase transformations. There are several methods to evaluate the activation energy associated with the precipitation processes, such as the methods of Ozawa [20] and Kissinger [21]. In this paper, we applied the Kissinger method, according to which the equation can be expressed as:

$$\ln \frac{\Phi}{T_P^2} = -\frac{Q}{RT_P} + C_2 \quad (1)$$

where Φ is the scanning rate, T_P is the peak temperature, Q is the activation energy, R is the gas constant, and C_2 is a constant. According to Eq. (1), the apparent activation energy was determined from the plots of $\ln \frac{\Phi}{T_P^2}$ vs. $\frac{1}{T_P}$.

Fig. 7 shows the variation of DSC traces as a function of the scanning rate performed on as-quenched sample. It indicates that the thermal effects shift toward higher temperatures as the heating rate increased. The relationship of $\ln \frac{\Phi}{T_P^2}$ vs. $\frac{1}{T_P}$ is shown in Fig. 8 and the calculated apparent activation energies for the β′ and β_1/β precipitation are presented in Table 1.

The activation energy for the β′ precipitation was determined to be 104 kJ/mol, which was lower than the activation energy for lattice diffusion of Mg (135 kJ/mol) [22]. Although few data of acti-

Table 1
Apparent activation energies for different processes.

Process	Signal	Apparent activation energy (kJ/mol)
β′ Precipitation	B	104
β_1/β Precipitation	C	172

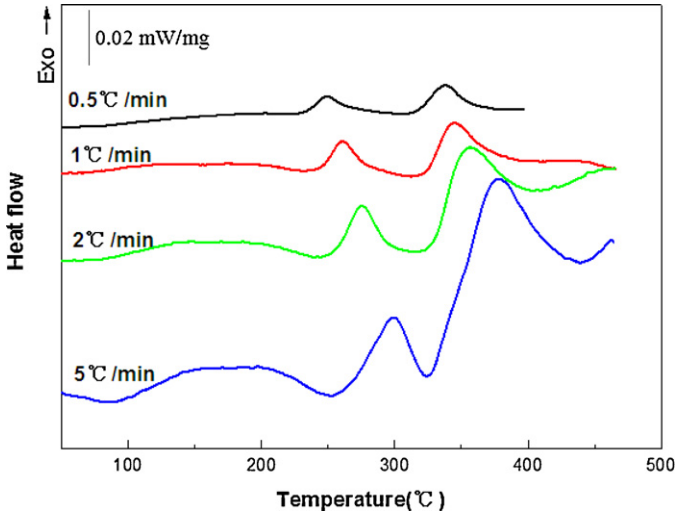

Fig. 7. DSC traces after baseline subtraction of the as-quenched samples with different scanning rates.

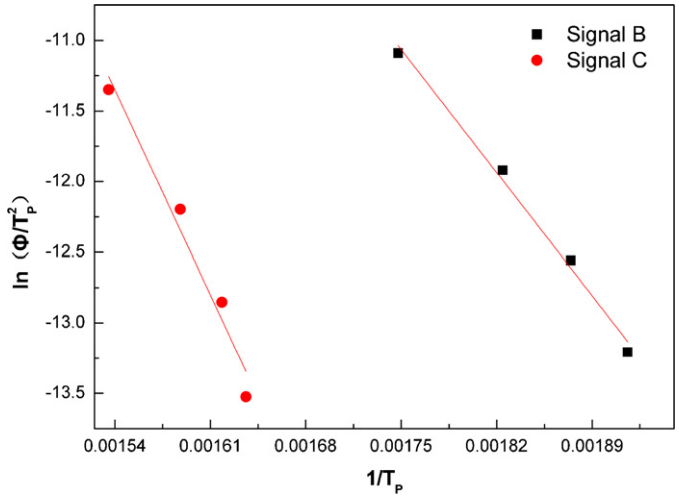

Fig. 8. $\ln \frac{\Phi}{T_P^2}$ as a function of $\frac{1}{T_P}$ for different processes.

vation energies for the diffusion of the rare earth elements Gd, Y and Nd in Mg are reported, it is noted that the atomic radii of Gd, Y, and Nd are 13%, 13% and 14% higher than that of Mg, respectively [23]. Hence, the possible mechanism for the β′ precipitation is the diffusion of rare earth atoms assisted by the abundant quench-in vacancies. In addition, it was found that the activation energy for the β_1/β precipitation was much higher than that of the β′ precipitation and approximately equal to the ones in other rare earth containing magnesium alloy [16]. Therefore, the rapid growth on hardness in the initial stage of the 215 °C-aged samples was ascribed to the fast formation of the β′ precipitates due to the low activation energy value for its formation. The wide hardness plateau from 16 h to 192 h may be due to the stability of the β′ phase because of the high activation energy for the transformation from the β′ to the β_1 and β phases.

4. Summary

DSC testing was carried out on samples with different initial states, and the phase transformations were related to the exothermic and endothermic signals in the DSC curves according to TEM observations. The results indicated the presence of the intermediate β_1 precipitate in Mg–8Gd–4Y–Nd–Zr alloy. The apparent activation energies for the precipitation of the β′ and β_1/β phases were determined to be 104 kJ/mol and 172 kJ/mol, respectively.

Acknowledgements

The authors would like to appreciate the financial supports from the National Basic Research Program, China.

References

[1] H.E. Friedrich, B.L. Mordike, Magnesium Technology: Metallurgy, Design Data, Applications, Springer, Berlin, 2006.
[2] G. Riontino, D. Lussana, M. Massazza, A. Zanada, J. Mater. Sci. 41 (2006) 3167.
[3] C. Antion, P. Donnadieu, F. Perrard, A. Deschamps, C. Tassin, A. Pisch, Acta Mater. 51 (2003) 5335.
[4] X. Gao, S.M. He, X.Q. Zeng, L.M. Peng, W.J. Ding, J.F. Nie, Mater. Sci. Eng. A 431 (2006) 322.
[5] J.F. Nie, B.C. Muddle, Scripta Mater. 40 (1999) 1089.
[6] Z. Yang, J.P. Li, Y.C. Guo, T. Liu, F. Xia, Z.W. Zeng, M.X. Liang, Mater. Sci. Eng. A 454–455 (2007) 274.
[7] P.J. Apps, H. Karimzadeh, J.F. King, G.W. Lorimer, Scripta Mater. 48 (2003) 1023.
[8] J.F. Nie, B.C. Muddle, Acta Mater. 48 (2000) 1691.
[9] J.F. Nie, Scripta Mater. 48 (2003) 1009.
[10] P.J. Apps, H. Karimzadeh, J.F. King, G.W. Lorimer, Scripta Mater. 48 (2003) 475.
[11] T. Honma, T. Ohkubo, K. Hono, S. Kamado, Mater. Sci. Eng. A 395 (2005) 301.
[12] T. Honma, T. Ohkubo, K. Hono, S. Kamado, Mater. Sci. Eng. A 404 (2005) 330.
[13] G. Riontino, M. Massazza, D. Lussana, P. Mengucci, G. Barucca, R. Ferragut, Mater. Sci. Eng. A 494 (2008) 445.
[14] P. Mengucci, G. Barucca, G. Riontino, D. Lussana, M. Massazza, R. Ferragut, E.H. Aly, Mater. Sci. Eng. A 479 (2008) 37.
[15] G. Riontino, D. Lussana, M. Massazza, G. Barucca, P. Mengucci, R. Ferragut, J. Alloys Compd. 463 (2008) 200.
[16] G. Riontino, D. Lussana, M. Massazza, J. Therm. Anal. Calorim. 83 (2006) 643.
[17] G. Barucca, R. Ferragut, D. Lussana, P. Mengucci, F. Moia, G. Riontino, Acta Mater. 57 (2009) 4416.
[18] S.M. He, X.Q. Zeng, L.M. Peng, X. Gao, J.F. Nie, W.J. Ding, J. Alloys Compd. 427 (2007) 316.
[19] E. Orowan, Inst. Met. (1948) 451.
[20] T. Ozawa, Poly 12 (1971) 150.
[21] H.E. Kissinger, J. Res. Nat. Bur. Stand. 57 (1956) 217.
[22] H.J. Frost, M.F. Ashby, Deformation Mechanism Maps, Pergamon Press, Oxford, 1982.
[23] L.L. Rokhlin, Magnesium Alloys Containing Rare Earth Metals: Structure and Properties, Taylor & Francis Eds, London, 2003.